Available online at www.sciencedirect.com
ScienceDirect
International Journal of Multiphase Flow 34 (2008) 461–476
International Journal of Multiphase Flow
www.elsevier.com/locate/ijmulflow

The characteristics of gas/liquid flow in large risers at high pressures

N.K. Omebere-Iyari [a,1], B.J. Azzopardi [a,*], D. Lucas [b], M. Beyer [b], H-M Prasser [c]

[a] Multiphase Flow Research Group, Nottingham Fuel and Energy Centre, School of Chemical, Environmental and Mining Engineering, University of Nottingham, University Park, Nottingham NG7 2RD, UK
[b] Forschungszentrum Dresden-Rossendorf e.V., Institute of Safety Research, P.O. Box 510 119, D-01314 Dresden, Germany
[c] Eidgenössische Technische Hochschule Zürich, Department of Mechanical and Process Engineering, ETH-Zentrum, CH-8092 Zürich, Switzerland

Received 24 January 2007; received in revised form 30 July 2007

Abstract

Although most of the work reported on two-phase flows are limited to small pipe diameters, two-phase flow in large risers are increasingly being encountered in the petroleum and nuclear industries. In the present work, a wire mesh sensor was employed to obtain void fraction and bubble size distribution data and visualizations of steam/water flow in a large vertical pipe (194 mm in diameter) at 46 bar. For comparison purposes, measurements were made at similar phase velocities and physical properties to a dataset for nitrogen/naphtha flow in a similar-sized riser. There exist significant differences between both sets of data. Churn-turbulent flow is observed in the present work instead of slug flow, and this differs from the intermittent and semi-annular flow patterns reported for nitrogen/naphtha data. The mean void fraction of the nitrogen/naphtha data is higher than that of the present steam/water data due to the differences in purity in the liquid phases. Furthermore, core peak distributions are observed for the present work in contrast to the flatter profiles deduced for the nitrogen/naphtha using a power law relationship.

Keywords: Two-phase flow; Large diameter; Vertical pipe; High pressure; Wire mesh sensor; Void fraction

1. Introduction

Applications involving two phase flows in large diameter pipes can be found in the power, process and petroleum industries. In offshore exploration, large risers are increasingly being applied to deepwater oil fields to reduce pressure drop. For nuclear reactors, Yoneda et al. (2002) reports that the operational performance of natural-circulation boiling water reactors depends on the flow characteristics of the riser whose diameter is the same as the core, i.e., about 6 m. However, despite the importance of large risers, most prediction methods for two-phase flow parameters such as flow pattern and void fraction are based on work from smaller pipes.

The very little work available in large diameter vertical pipes shows that two-phase flow characteristics vary from the established behaviour in smaller pipes. For instance, Omebere-Iyari et al. (2007) reports the absence of conventional slug flow for the flow of a nitrogen/naphtha mixture in a 189 mm diameter riser at 20 and 90 bar. This is contrary to previous investigations by many researchers, e.g. Taitel et al. (1980); Costigan and Whalley (1997), working with pipes of smaller diameters suggest that gas/liquid two-phase flow in vertical pipes exhibits bubble, slug, churn and annular flows with the increase of void fraction. Cheng et al. (1998) concluded that instead of traditional slug flow in their column, there is a very gradual transition to a type of churn flow as the gas rate is increased. However, they found that the void fraction fluctuated periodically. This was observed in the signals of cross-sectional averaged void fraction and point void fraction probes and is a behaviour

* Corresponding author. Tel.: +44 (0) 115 951 4160; fax: +44 (0) 115 951 4115.
E-mail address: barry.azzopardi@nottingham.ac.uk (B.J. Azzopardi).
[1] Present address: Granherne Ltd., Kellogg, Brown and Root (KBR), Leatherhead KT22 7LH, UK.

0301-9322/$ - see front matter © 2007 Elsevier Ltd. All rights reserved.
doi:10.1016/j.ijmultiphaseflow.2007.11.001

associated with intermittent flows. Investigations by Ohnuki and Akimoto (2000) into upward air/water flow along a large diameter pipe (200 mm) found that churn flow is dominant in the large diameter pipe under the conditions where small-scale pipes have slug flow. The flow patterns observed were classified as undisturbed bubbly, agitated bubbly, churn bubbly, churn slug and churn froth. Using a wire mesh sensor, Prasser et al. (2005a) obtained virtual side projections for air/water flow in a 194 mm pipe confirming the visual observations of Ohnuki and Akimoto (2000). In experiments performed by Kobayashi et al. (2004), the classical, bullet shaped Taylor bubbles were absent and the observed flow patterns were similar to those obtained by Ohnuki and Akimoto (2000). Kytomaa and Brennen (1991) in their work with air and water in a 102 mm diameter column, found a transition from bubbly flow to churn-turbulent flow rather than to slug flow. There exists therefore, a strong possibility that slug flow does not actually exist in large diameter pipes in the form envisaged by the most commonly used flow pattern maps. Later work by Hibiki and Ishii (2000), Shoukri et al. (2003) and Zhu et al. (2004) corroborates the absence of conventional slug flows in large diameter pipes.

The present work describes detailed measurements of steam/water flow in the same 194 mm diameter vertical pipe as employed by Prasser et al. (2005a). The present data is taken at 46 bar and at similar flow rates to the work reported by Omebere-Iyari et al. (2007) for comparison purposes. The pressure has been chosen to give equivalent physical properties as the work of Omebere-Iyari et al. (2007) at 20 bar. A wire mesh sensor was used to obtain high speed visualisation of transient spatial structures and to make measurements of void fraction and phase distribution to augment our understanding of two-phase flow behaviour in large vertical pipes.

2. Experimental arrangement

2.1. Flow loop

The present experiments were carried out at the TOPFLOW (transient two phase flow) facility within the Institute of Safety Research, FZD, Germany. A flowsheet of the TOPFLOW facility is given in Fig. 1. Measurements were made at 46.4 bar on the vertical test section 1 of TOPFLOW, which is 9 m in height and 194 mm in diameter. The fluids employed were steam and water. Water is supplied from the steam drum to the vertical pipe by the test section pump. The steam is produced in the heat source section which consists of an electric heater, circulation pump and cyclone separator. The flow measurements were made using multi-strand nozzle meters with a maximum error of 1% over the range of the present measurements (Prasser et al., 2005b). Steam is introduced to the test section through a specially designed mixing section and injection points at the bottom of the pipe. The two phases then

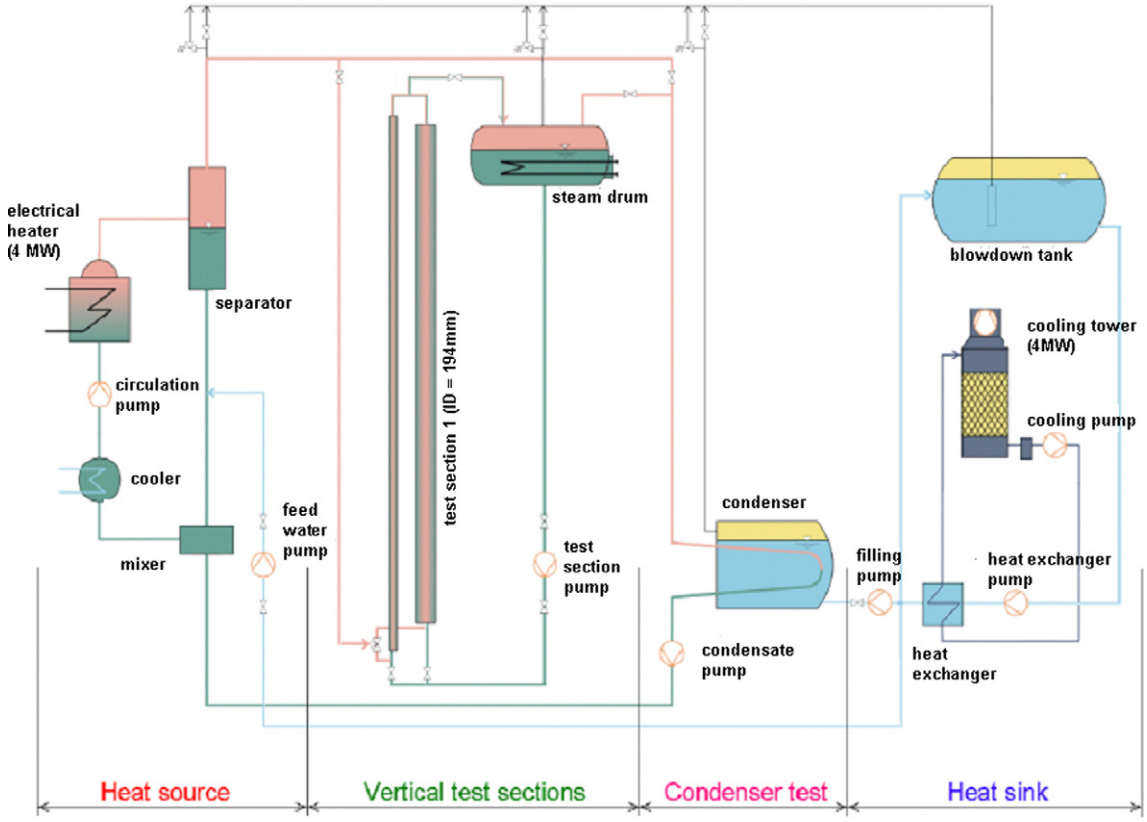

Fig. 1. Flowsheet of the TOPFLOW facility.

travel vertically upwards and thereafter the mixture flows into the steam drum where separation occurs. Measurements were made using a wire mesh sensor positioned at 7.6 m from the mixer. The water exits the bottom of the drum to be re-introduced to the test section. The steam either condenses in the drum or is diverted to the blow down tank.

This experimental set-up is unique as there are limited data from test facilities of this magnitude in the literature. Although Okawa et al. (1999) reports large-scale steam/water experiments at high pressures, their L/D ratio is limited to 4.2 and the maximum pressure obtained is 5 bar, far less that what is obtainable on TOPFLOW.

2.1.1. Mixing configuration

The mixing device consists of 8 branches with 12× 0.8 mm holes and 8 branches with 7 × 0.8 mm holes. The facility has the possibility of variable gas injection methods to study flow development. This is illustrated in Fig. 2. For the present experiments, a combination of the porcupine mixer and the P and R injection points from the variable mixing configuration are used to introduce the gas phase.

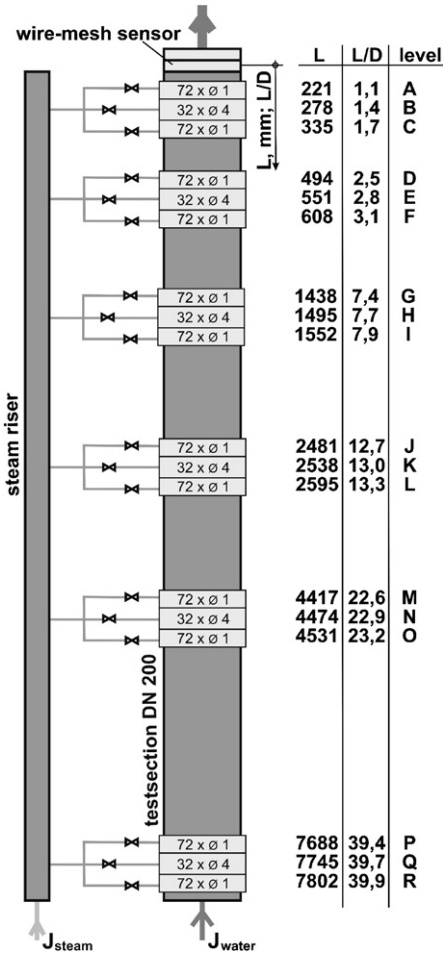

Fig. 2. Large vertical test section (194 mm diameter) of the TOPFLOW facility showing variable gas injections.

The P and R injection points have 72, 1 mm diameter holes each.

2.1.2. Physical properties of fluids

The present measurements were made for a saturated steam and saturated water mixture at 46.4 bar and 259.3 °C. At this condition, the gas density and viscosity are equal to the 20 bar data of Omebere-Iyari et al. (2007) while the liquid density, surface tension and liquid viscosity are 1.2, 1.3 and 0.3 times that employed in the above mentioned work. This enables both sets of data to be compared. The physical properties are given in Table 1.

2.2. Wire mesh sensor measurements

The development of an electrode mesh tomograph for high speed visualisation of two-phase flows based on measurements of local instantaneous conductivity is presented by Prasser et al. (1998). The current sensor is an improved version reported by Pietruske and Prasser (2005), for application to steam/water flows at pressures of up to 70 bar. The sensor is shown in Fig. 3.

Cross-section averaged void fraction, bubble size distribution and radial profile are extracted from the raw data by the methods described by Prasser et al. (2001, 2002).

Table 1
Relevant fluid properties

		Units	Present work	Omebere-Iyari et al. (2007)
Fluid pairing		–	Steam/water	Nitrogen/naphtha
Pipe diameter		mm	194	189
Temperature/ pressure		bar/°C	46.4/259.3	20/30
Density	Gas	kg/m^3	23.4	23.4
	Liquid	kg/m^3	784.9	702.3
Viscosity	Gas	Gas (Pa s)	1.79E−05	1.77E−05
	Liquid	Liquid (Pa s)	1.03E−04	3.59E−04
Surface tension		(N/m)	0.0239	0.0185

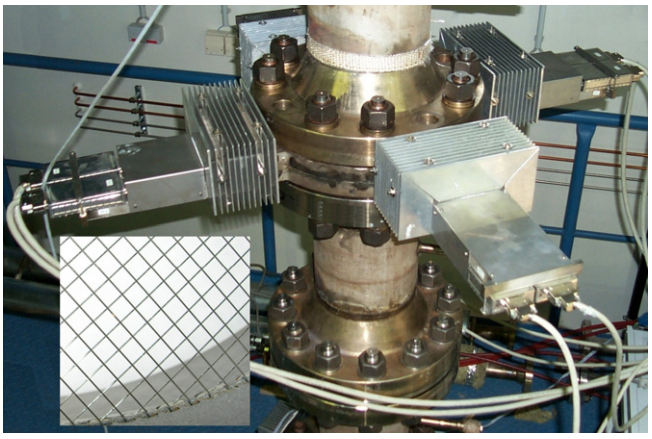

Fig. 3. Wire mesh sensor installed in the pipe. The inset is the top view of the mesh grid.

The void fraction matrix can be visualized from the measuring plane, virtual sectional side views and virtual side projections as described by Prasser et al. (2005a).

2.2.1. Principle of operation

The operating principle of the wire mesh technique is based on a considerable difference in the electrical conductivities of the fluid pair employed. In the present experiments, the relative electrical conductivity of water in comparison to steam is significant. The wire mesh sensor yields a sequence of instantaneous conductivities in each junction formed by a pair of crossing wires (a transmitter wire, i and a receiver wire, j). For each measuring location, the instantaneous gas fraction is determined by relating the two-phase conductivity to the reference signal for the liquid phase only. This gives a three-dimensional matrix of void fractions, $\alpha_{i,j,k}$, where k is the number of measurements, i and j correspond to a pair of crossing electrode wires (transmitter and receiver). The sensor consists of 64 receiver and 64 transmitter wires of 250 mm diameter, which gives a measuring matrix with 64×64 elements. The distance between the wires is 3 mm and the inner diameter of the sensor is equivalent to the test section. During signal acquisition, voltage pulses are supplied successively to activate the transmitter wires or electrodes. The resulting current at the receiver wire due to this transmission is a measure of the fluid conductivity in the control volume surrounding the junction of the two wires. The sensor operates at a frequency of 2500 frames/s which enables small bubbles to be identified.

2.3. Gamma densitometry

Omebere-Iyari et al. (2007) used two types of gamma-ray densitometers in their two-phase flow experiments. The gamma densitometers employ a Cs 137 radioactive source which emits gamma rays on one side of the pipe to be picked up on the other side by an ionization type detector. As the gamma rays are attenuated differently in gas and liquid, the radiation intensity at the detector depends on the phase distribution in the pipe. With the signals for pure gas and liquid as reference points, the densitometers give a direct measure of the ray path occupied by liquid or gas.

Fig. 4 shows the two types of gamma densitometers employed. Broad beam and single beam densitometers were used to measure cross-sectionally and line averaged void fraction, respectively. For the broad beam instrument, the gamma beam diameter (d_{gamma}), is equal to the pipe diameter while in the case of the single beam densitometer this is 25 mm. From geometry, we estimate that for the broad and single beam densitometers, the axial length of the gamma ray in the pipe flow (h_{gamma}) are 100 and 25 mm, respectively.

2.4. Flow rates and heat balance

In the present experiments, measurements were made at exactly the same inlet phase velocities as some of the data from the work of Omebere-Iyari et al. (2007). The highest gas superficial velocity achieved here is 1.5 m/s because of

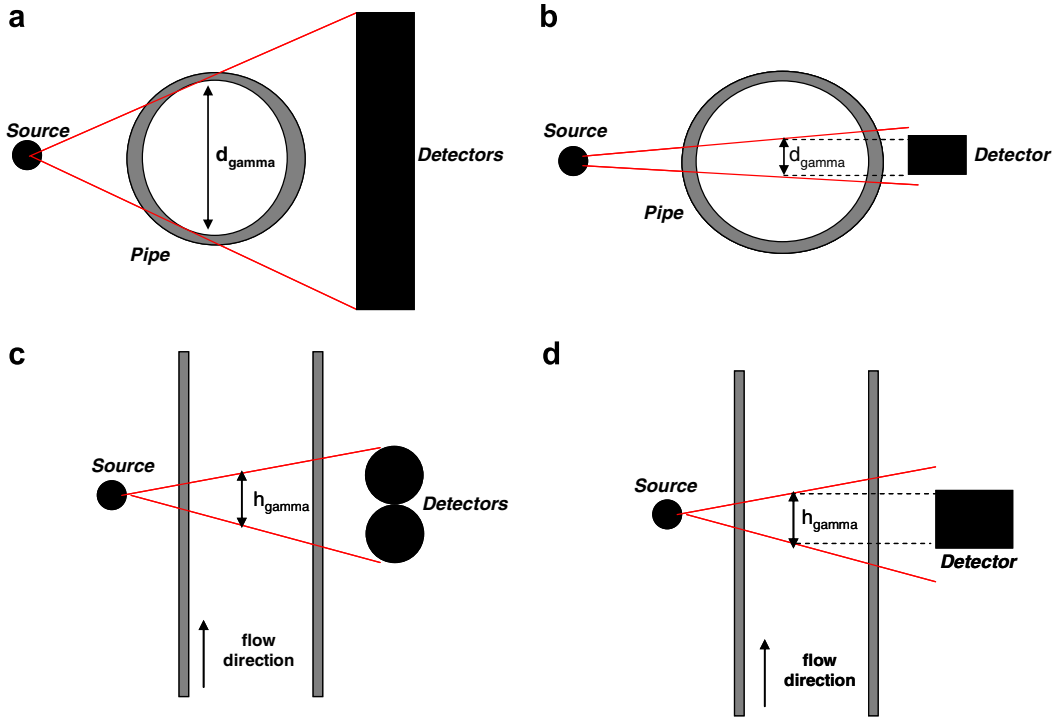

Fig. 4. Schematic diagram showing operation of gamma densitometers, (a) top view of broad beam instrument, (b) top view of single beam instrument, (c) broad beam instrument in axial direction, (d) single beam instrument in axial direction.

limitations with the power supply required for steam generation.

A heat balance of the flow streams (Fig. 5) is required to determine the actual flow rates of the gas and liquid phases at the wire mesh sensor. This is to account for condensation which occurs as the two-phase flow mixture travels up the pipe. The estimation is achieved by using the inlet temperatures, pressures and flowrates and the temperature and pressure at the wire mesh sensor. Assuming equilibrium of the two-phases at the sensor

$$M_{v1}h_{v1} + M_{L1}h_{L1} = (M_{v2} - x)h_{v2} + (M_{L2} + x)h_{L2} + \dot{Q}_{\text{loss}} \tag{1a}$$

$$x = \frac{(M_{v1}h_{v1} + M_{L1}h_{L1}) - (M_{v2}h_{v2} + M_{L2}h_{L2}) - \dot{Q}_{\text{loss}}}{(h_{L2} - h_{v2})} \tag{1b}$$

where x is condensed steam in kg/s, M is mass of liquid or gas in kg/s, h is enthalpy in kJ/kg, $\dot{Q}_{\text{loss}}$ is heat loss in kW, v denotes vapour and L is liquid. T denotes temperature and P is the pressure. The subscripts 1 and 2 denote the conditions at the inlet and the sensor, respectively. U_{GS} and U_{LS} are the superficial gas (or vapour) and liquid velocities, respectively.

Heat loss is taken to be 4 kW based on previous tests on the TOPFLOW facility. This value is very small in comparison to the enthalpies involved and its effect is negligible. The phase velocities on entry to the test section and at the wire mesh sensor together with other results from the heat balance are given in Table 2. The amount condensed is largest for the highest liquid inlet flow rates

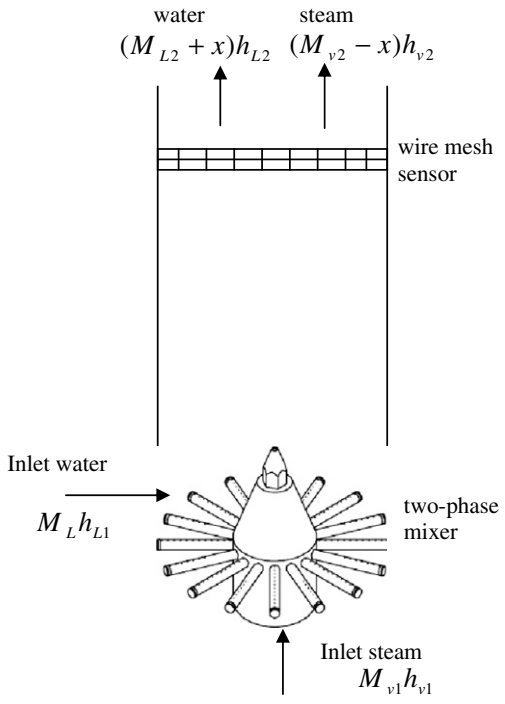

Fig. 5. Schematic diagram showing mixer and heat balance in the test section.

Table 2
Results from the heat balance

U_{GS1} (m/s)	U_{LS1} (m/s)	M_{v1} (kg/s)	M_{L1} (kg/s)	T_{v1} (°C)	P_{v1} (bar)	h_{ev1} (kJ/kg)	T_{L1} (°C)	P_{L1} (bar)	h_{eL1} (kJ/kg)	T_2 (°C)	P_2 (bar)	h_{ev2} (kJ/kg)	h_{eL2} (kJ/kg)	x_s (kg/s)	Condensed (%)	U_{GS2} (m/s)	U_{LS2} (m/s)
0.21	0.10	0.145	2.311	259.0	47.1	2796.4	254.9	46.7	1111.0	257.9	46.2	2797.1	1125.5	0.023	15.5	0.18	0.10
0.29	0.10	0.200	2.309	259.2	47.3	2796.3	254.9	46.5	1111.0	257.7	46.0	2797.2	1124.7	0.021	10.7	0.26	0.10
0.34	0.10	0.234	2.313	259.9	47.8	2795.9	254.9	46.8	1111.0	258.1	46.3	2797.0	1126.7	0.024	10.4	0.30	0.10
0.41	0.10	0.280	2.311	259.5	47.5	2796.1	255.2	46.8	1112.4	257.9	46.1	2797.1	1125.5	0.021	7.4	0.38	0.10
0.50	0.10	0.344	2.319	260.2	48.0	2795.7	255.9	46.5	1115.9	257.7	46.0	2797.2	1124.9	0.015	4.4	0.48	0.10
0.69	0.10	0.480	2.315	263.0	50.2	2794.0	252.9	46.5	1101.2	257.9	46.2	2797.1	1125.5	0.037	7.7	0.64	0.10
1.01	0.10	0.696	2.315	268.5	54.8	2789.9	253	46.7	1101.6	258.2	46.4	2796.9	1127.2	0.041	5.9	0.95	0.10
0.19	0.65	0.131	15.056	259.1	47.1	2796.3	256.7	46.8	1119.8	258.0	46.2	2797.0	1126.0	0.058	44.5	0.11	0.65
0.50	0.65	0.347	15.057	260.6	48.3	2795.5	257	46.8	1121.3	258.0	46.2	2797.0	1126.1	0.046	13.2	0.44	0.65
1.01	0.65	0.695	15.050	268.6	54.9	2789.8	257	46.5	1121.3	257.9	46.2	2797.1	1125.6	0.044	6.3	0.94	0.65
0.10	0.01	0.067	0.230	258.6	46.8	2796.6	251.5	46.6	1094.3	257.7	46.1	2797.1	1124.8	0.007	9.9	0.09	0.01
0.16	0.01	0.110	0.231	258.8	46.9	2796.5	252.9	46.7	1101.2	257.9	46.1	2797.1	1125.7	0.006	5.3	0.15	0.01
0.21	0.01	0.145	0.231	258.9	47.1	2796.4	254.5	46.7	1109.0	257.9	46.1	2797.1	1125.7	0.005	3.3	0.20	0.01
0.49	0.01	0.335	0.231	260.2	47.9	2795.8	249.6	46.4	1085.1	257.7	46.0	2797.1	1124.6	0.008	2.4	0.47	0.01
0.99	0.01	0.684	0.231	268.0	47.1	2790.3	247.9	46.5	1076.8	257.9	46.2	2797.0	1125.9	0.012	1.7	0.97	0.01
1.51	0.01	1.045	0.232	279.6	47.3	2778.6	246.3	47.0	1069.0	258.6	46.8	2796.6	1129.3	0.022	2.1	1.48	0.01

where a small amount of sub-cooled liquid has a greater effect on the heat balance.

3. Results

3.1. Flow development

Previous measurements of bubble size distribution and radial void fraction profile on the TOPFLOW facility for a steam/water mixture at 40 bar were examined to determine the extent of flow development. The L/D (pipe length/diameter) ratios ranged from 1.4 to 39.7 (Fig. 2). The results in Table 3 show that at an L/D of 7.7 the flow is fully developed. The bubble size distributions and radial profiles at this and subsequent locations are equivalent, suggesting that equilibrium has been reached. This means that the present experiments which are conducted at an L/D ratio of approximately 40 are fully developed. This

Table 3
Examination of flow development using radial void fraction profiles and bubble size distributions at 40 bar

Gas superficial velocity (m/s)	Radial void profile	Bubble size distribution
0.53	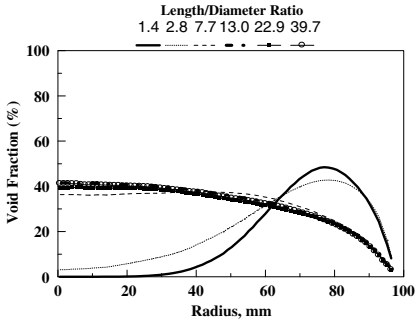	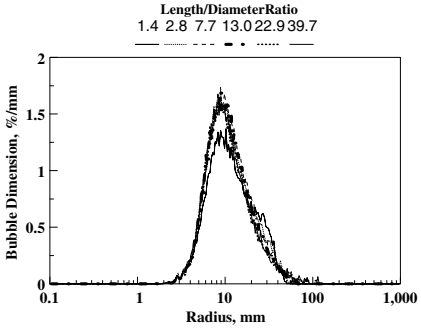
1.31	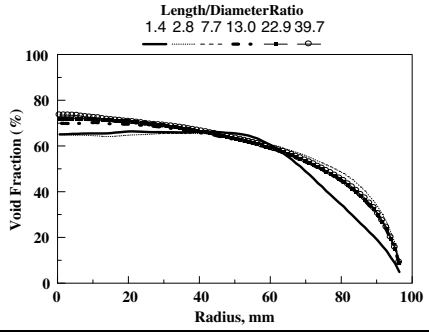	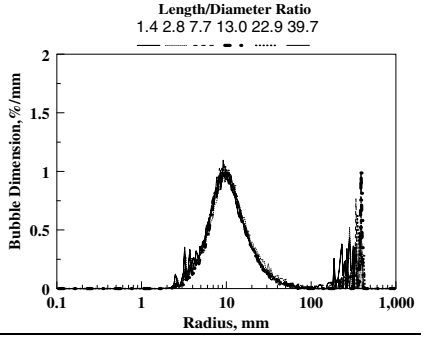

The liquid superficial velocity is 1 m/s.

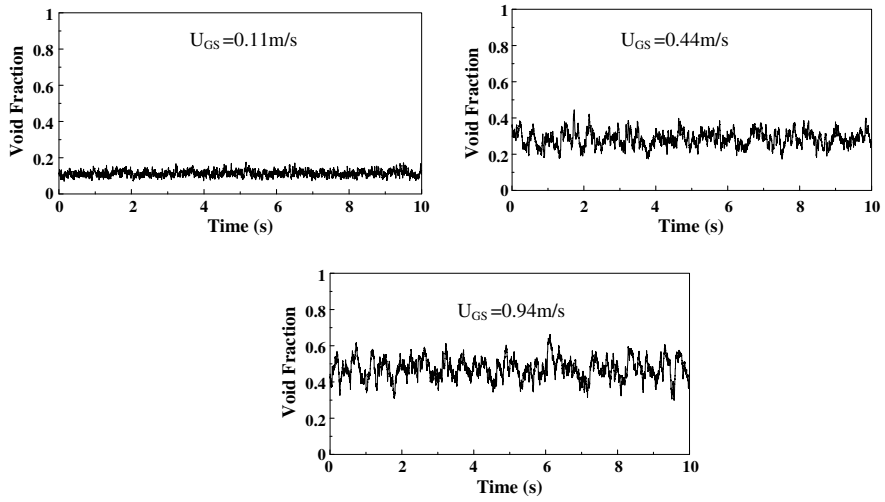

Fig. 6. Raw time varying, cross-section averaged void fraction at a constant liquid superficial velocity of 0.65 m/s for various gas superficial velocities.

is consistent with Prasser et al. (2005c), who observe that two-phase flow involving steam/water mixtures at 65 bar converges much quicker than air/water mixtures under atmospheric conditions but different to Omebere-Iyari et al. (2007) who found that an L/D of 157 is required for fully developed flow of a nitrogen/naphtha mixture in a similar-sized pipe to the present experiments.

3.2. Void fraction

Prasser et al. (1998) have shown that the void fraction measurements obtained from a conductance wire mesh sensor and a gamma densitometer are consistent. A simple moving average procedure (described in the Appendix) is implemented to align the wire mesh data in time and height with the measurements of the gamma densitometer due to differences in the data acquisition frequency and resolution of both instruments. This ensures that comparisons between the present steam/water data and the nitrogen/naphtha data of Omebere-Iyari et al. (2007) are not influenced by the measurement technique applied.

3.2.1. Cross-sectionally averaged void fraction

The cross-section averaged void fractions show a direct transition from the characteristic low values of bubble flow to the large void fluctuations present in churn-turbulent flow, for all liquid flow rates studied. Fig. 6 shows representative time-varying void fraction plots which illustrate such a transition at the liquid superficial velocity of 0.65 m/s for gas superficial velocities of 0.11, 0.44 and 0.94 m/s.

The present time varying void fraction and PDF plots for steam/water flow are compared with those from the nitrogen/naphtha tests of Omebere-Iyari et al. (2007) at 20 bar for similar phase velocities (Figs. 6 and 7). Fig. 7 shows reasonable agreement between void fraction values at the liquid superficial velocity of 0.65 m/s for both sets of data. However strong and systematic disparity at the lower liquid superficial velocity of 0.1 m/s is observed between the present work and that of Omebere-Iyari et al. (2007) in Fig. 8. The changes in the void fraction distribution as given by the PDF plots are also significantly different. At the liquid superficial velocity of 0.65 m/s in the nitrogen/naphtha tests, the PDF distribution is for bubble flow and shows very little transformation with an increase in gas flow rate. However, for the present steam/water tests, the PDF is characterised by broader distributions at similar phase velocities which represent churn-turbulent flow. In the case of the low liquid superficial velocity (0.1 m/s), the nitrogen/naphtha data exhibits bubble, intermittent and semi-annular flows as the gas flow rate is increased. Bubble flow for the nitrogen/naphtha data which is characterised by a single PDF peak at void fractions of less than 0.68 is present at the gas superficial velocities of 0.21, 0.29 and 0.34 m/s in Fig. 8. At the gas superficial velocities of 0.40 and 0.50 m/s, an intermittent flow pattern possessing two closely spaced PDF peaks which are absent in the steam/water experiments is observed. The gas superficial velocities of 0.64 m/s and 1 m/s for the nitrogen naphtha data are cases of semi-annular flow. However, the steam/water

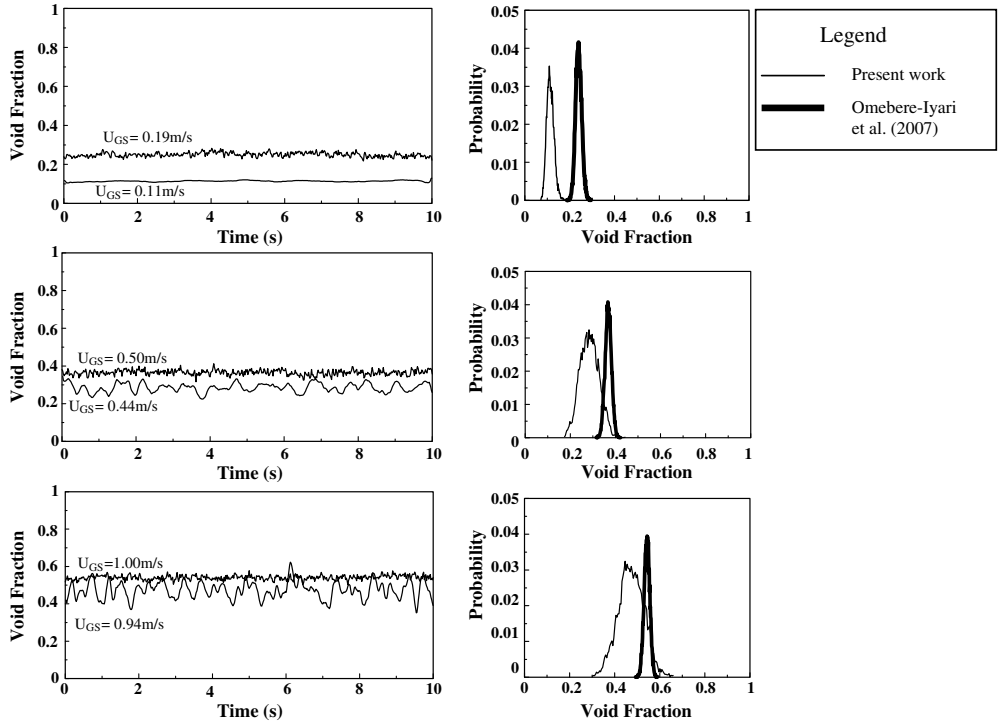

Fig. 7. Time varying, cross-sectional-averaged void fraction and PDF plots for a liquid superficial velocity of 0.65 m/s at similar gas superficial velocities for the present work (moving average applied) and the data of Omebere-Iyari et al. (2007).

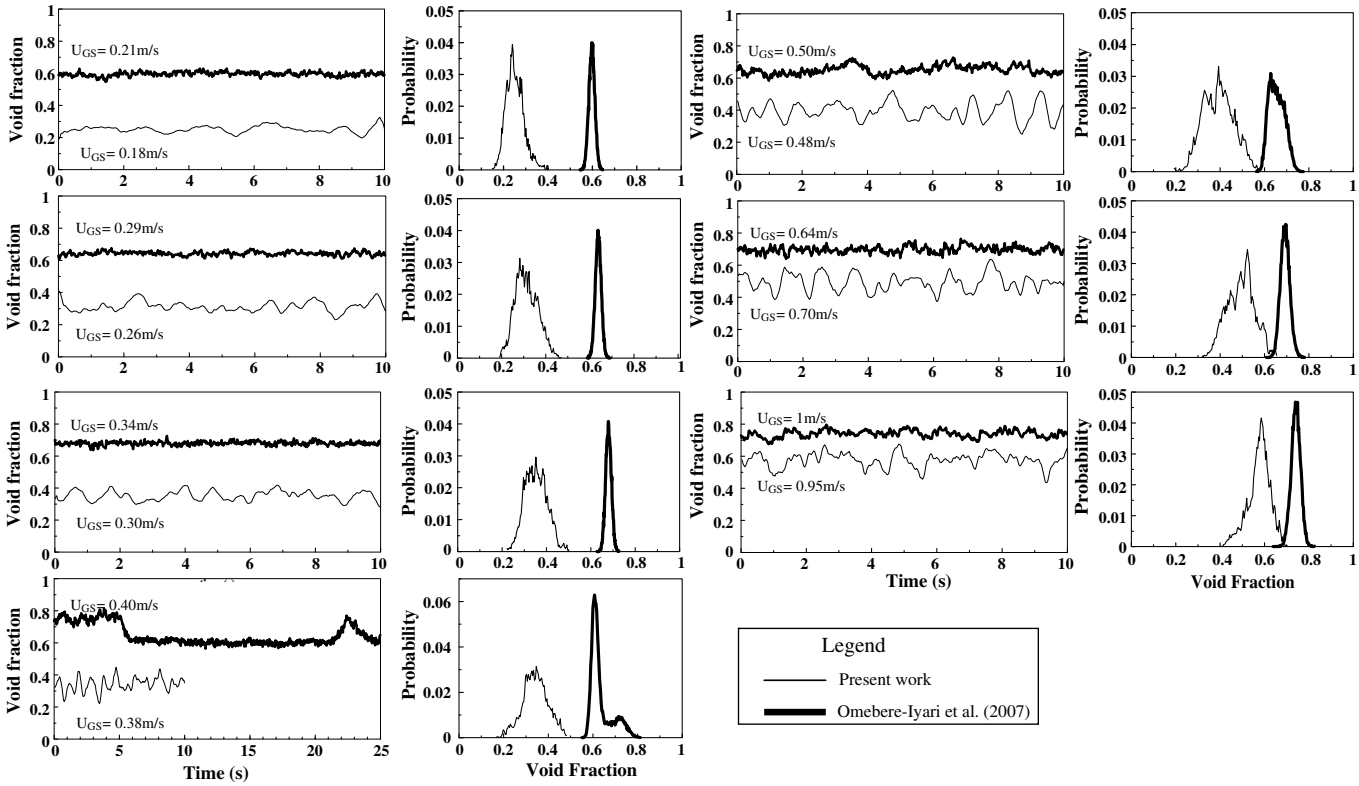

Fig. 8. Time varying, cross-sectional averaged void fraction and PDF plots for a liquid superficial velocity of 0.1 m/s at similar gas superficial velocities for the present work (after application of moving average) and Omebere-Iyari et al. (2007) data.

data in Fig. 8 shows a transition from bubble to churn-turbulent flow.

3.2.2. Line-averaged void fraction

Line-averaged void fraction was measured at two symmetrical axes in the work of Omebere-Iyari et al. (2007) with single beam gamma densitometers. Similar information has been extracted from the wire mesh sensor in the present experiments for comparison purposes. The measurement area in the centre of the pipe cross section is approximately equal to a rectangle with dimensions of 25 mm × 200 mm for both the wire mesh sensor and gamma densitometer. Fig. 9 illustrates the two measurement axes. The graph shows that the mean line void fraction for both axes is equivalent for the gamma densitometers and the wire mesh sensor.

The simple moving average method is also applied to the present time varying, line void fraction data for comparisons with the nitrogen/naphtha measurements of Omebere-Iyari et al. (2007) at 20 bar and for similar phase velocities. These are presented along with corresponding Probability Density Function (PDF) plots of the raw line void fraction data for the liquid superficial velocity of 0.1 m/s (Fig. 10). The present steam/water data shows more fluctuations than the nitrogen/naphtha results of Omebere-Iyari et al. (2007). These findings are in agreement with the comparisons of cross section-averaged void fraction.

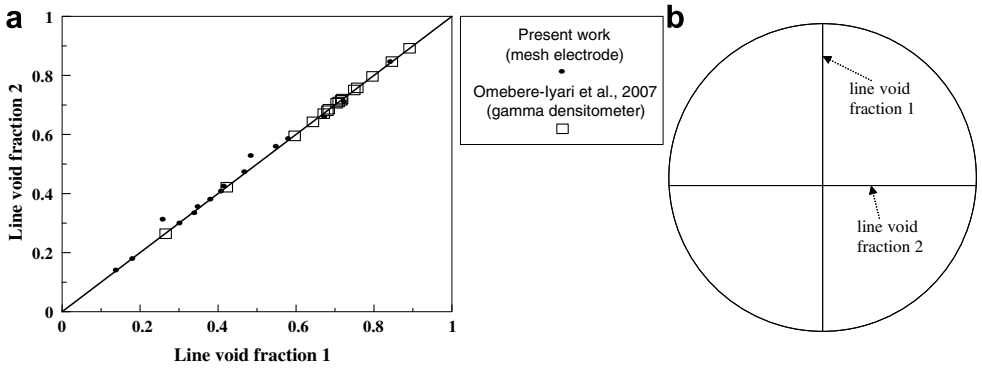

Fig. 9. Comparison of line void fraction data (a) and illustration of measurement configurations (b).

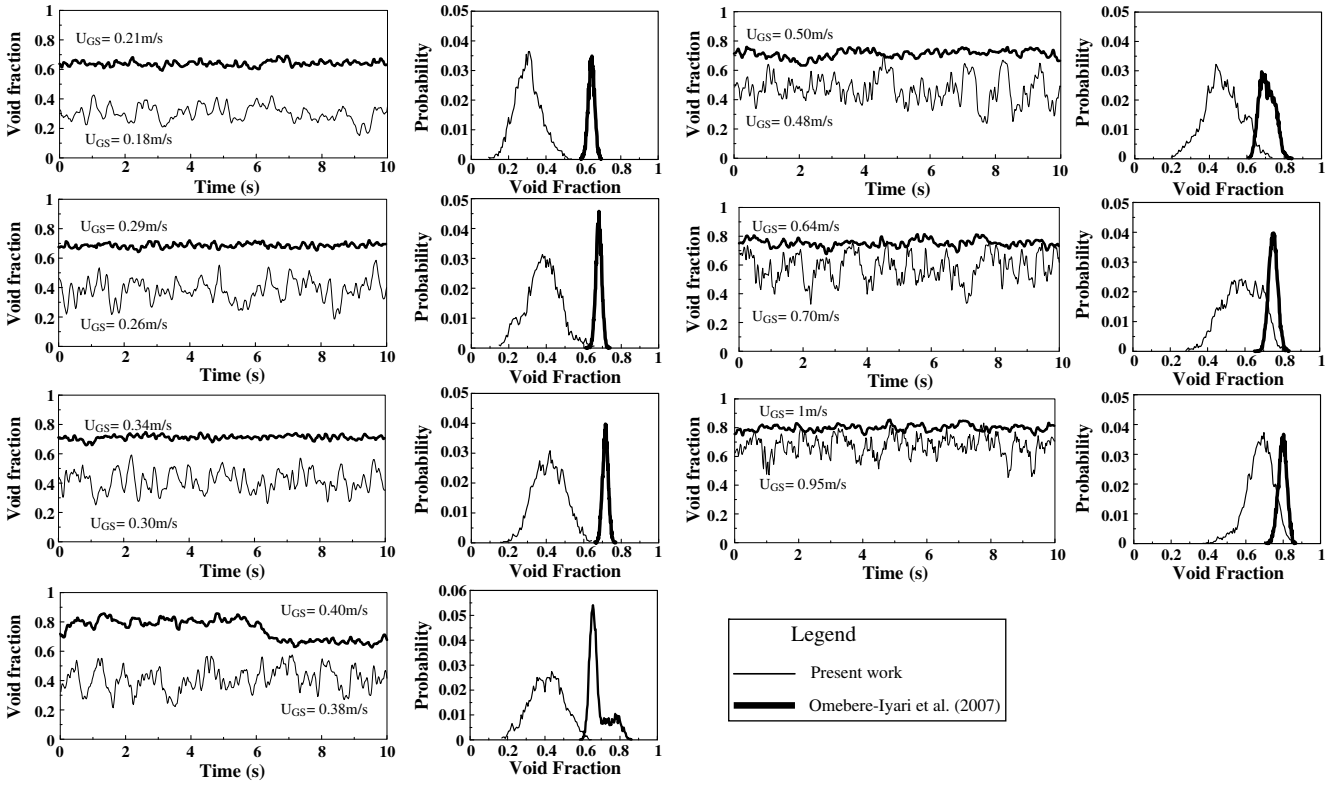

Fig. 10. Line void fraction and PDF for liquid superficial velocity of 0.1 m/s at similar gas superficial velocities for the present work (after application of moving average) and the data of Omebere-Iyari et al. (2007).

3.3. Flow pattern observations

The visual representations given in Fig. 11 of virtual side projections and sectional side views confirm the findings of Ohnuki and Akimoto (2000) and Prasser et al. (2005a) regarding the absence of conventional slug flow in pipes of similar diameter to that employed in the present tests. The sectional side views reveal the flow structure much

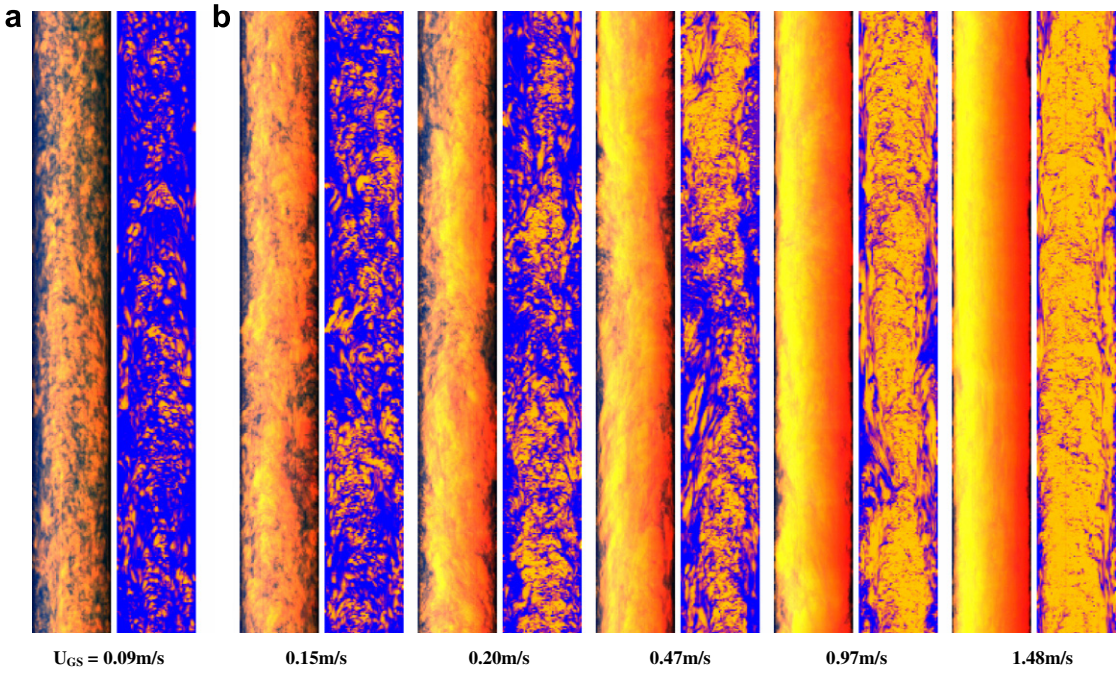

Fig. 11. Virtual side projections (a) and sectional side views (b) for liquid superficial velocity of 0.01 m/s.

better than the virtual side projections as they present the flow in the mid-plane of the pipe where bubbles close to the pipe wall are unable to obstruct viewing angles. Visualizations of sectional side views are used to classify the flow patterns in the steam/water experiments as either bubble or churn-turbulent. The classification method is illustrated in Fig. 12. Bubble flow is characterised by small bubbles in a liquid continuum while churn-turbulent flow is identified by large coalescent bubble clusters whose axial length is much greater than the pipe diameter.

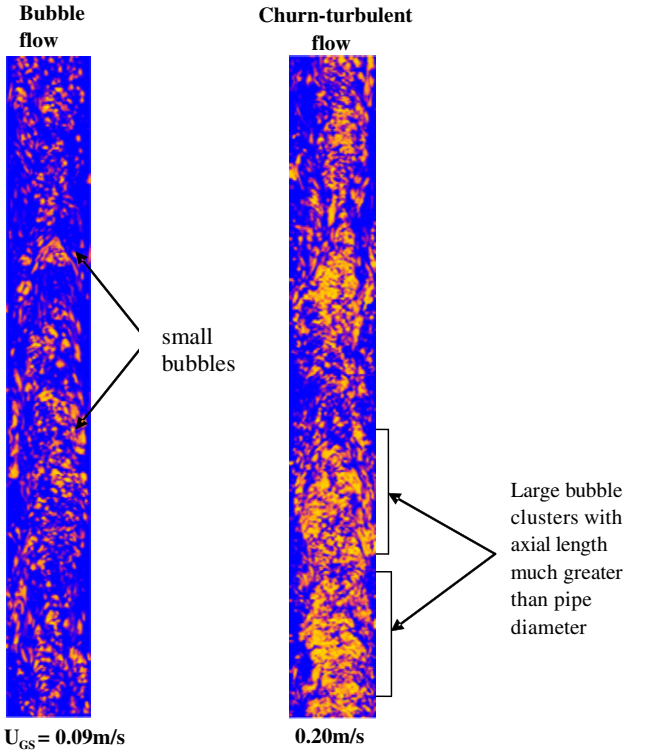

Fig. 12. Flow pattern classification using visualizations from the wire mesh sensor at a liquid superficial velocity of 0.01 m/s.

Fig. 11 shows small bubbles dispersed in the liquid continuum at the lowest gas flow rates. The magnitude of these bubbles grows with a corresponding increase in the gas flow rate. As the bubbles become larger and more irregular, the flow pattern changes to churn-turbulent. At the liquid superficial velocities of 0.01 m/s, the onset of this transition is observed at the gas superficial velocity of 0.20 m/s.

3.4. Bubble size distributions

The spatial resolution of the wire mesh sensor signal makes it possible to identify individual bubbles. A bubble is a region of interconnected gas containing elements of the data array, $\alpha_{i,j,k}$ that is surrounded by elements filled with the liquid phase. The bubble identification operation is described by Prasser (2004). In the present work, the bubble size is characterized by the diameter of a circle (D_{xy}) equivalent to the maximum area occupied by the bubble in the measuring plane during its passage through the sensor. Bubble size distributions are constructed by integrating the gas fraction carried by each individual bubble over classes of bubble diameters. The resulting histogram (H_{bub}) defined in Eq. (2), represents distributions of the partial void fraction over the bubble diameter.

$$H_{\text{bub}} = \frac{\Delta\varepsilon}{\Delta D_{xy}} = f(D_{xy}), \quad [\%/\text{mm}] \tag{2}$$

Typical bubble size distributions and radial void fraction profiles for the present TOPFLOW experiments are given in Fig. 13. Core peak profiles are observed for all the exper-

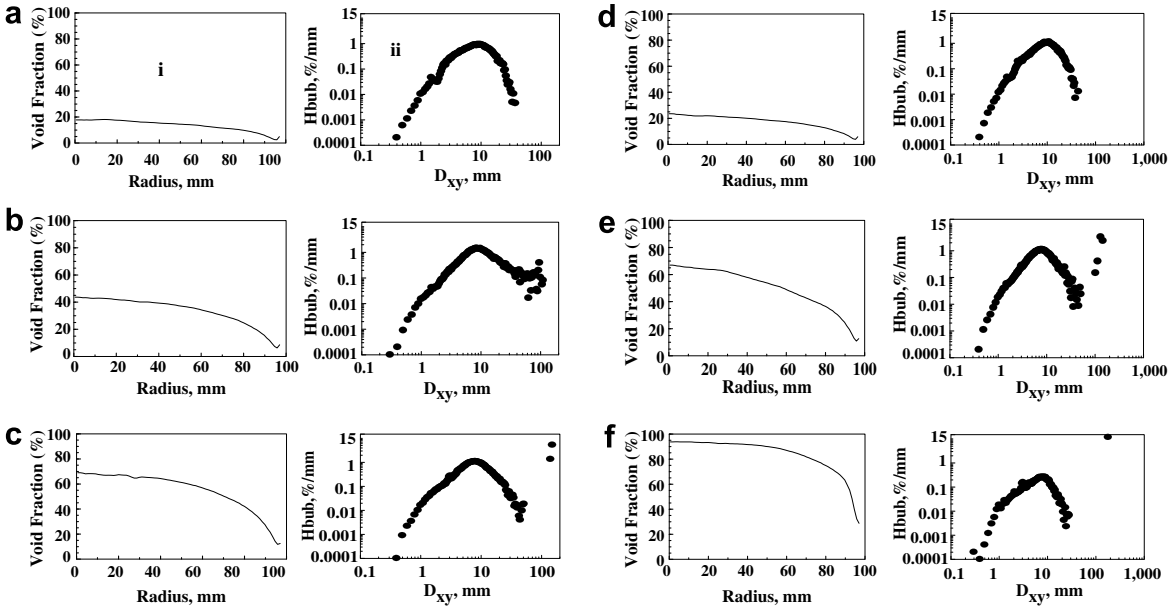

Fig. 13. Selected radial void fraction profiles (i) and bubble size distributions (ii) for the present steam/water experiments with the following respective gas and liquid superficial velocities in m/s: 0.11, 0.65 (a); 0.44, 0.65 (b); 0.94, 0.65 (c); 0.09, 0.01 (d); 0.47, 0.01 (e); 1.48, 0.01 (f).

iments. The bubble size distributions generally possess a peak around 10 mm at low gas flow rates corresponding to small bubbles. At the gas superficial velocities of 0.47, 0.94 and 1.48 m/s, bubble coalescence results in few large bubbles being observed (Fig. 13). As the horizontal bubble diameter is limited by the pipe diameter, the maximum size of these large bubbles is capped at about 200 mm.

4. Discussion

4.1. Drift flux

Zuber and Findlay (1965) proposed the two-phase flow drift flux model as

$$U_g = \frac{U_{gs}}{\varepsilon_g} = C_0(U_m) + U_{gd} \quad (3)$$

where U_g, U_{gs}, ε_g, C_0, U_m and U_{gd} are gas velocity, gas superficial velocity, void fraction, distribution coefficient, mixture velocity and drift velocity, respectively. The drift velocity and distribution coefficient are given by the slope and y-intercept respectively of the plot of gas velocity versus mixture superficial velocity.

The drift flux relationship for the present work is compared to the work of Shen et al. (2004) and Omebere-Iyari et al. (2007) in Fig. 14. This comparison is motivated by the fact that the data of Shen et al. (2004) is obtained for air/water flow in a similar-sized (200 mm diameter) vertical pipe at an L/D ratio of 113. Hence, the work by Shen et al. (2004) straddles the present work and the measurements by Omebere-Iyari et al. (2007), which are taken at L/D ratios of 39 and 207 respectively. The results of Shen et al. (2004) are consistent with the present steam/water data but are different from the nitrogen/naphtha data of Omebere-Iyari et al. (2007) even for similar phase velocities.

Fig. 15 shows the average drift velocities for the steam/water (present work) and the nitrogen/naphtha (Omebere-Iyari et al., 2007) experiments. At the liquid superficial velocity of 0.1 m/s, the drift velocities of the steam/water and nitrogen/naphtha data are 0.44 and −0.04 m/s respectively. This disparity is consistent with the significant difference in the line and cross-section averaged void fraction from the nitrogen/naphtha data and the steam/water tests. Negative drift velocities may develop in large pipes when there is a low net liquid flowrate (such as for the aforementioned cases) because fluid recirculation which are local in space and time can occur. Furthermore, negative drift velocities are also possible in wall peak phase distributions as small bubbles moving in the axial flow direction can also be transported from the centre of the pipe to the walls. This significantly decreases the net drift motion in the axial flow direction and contributes to a reduction in the one-dimensional drift velocity.

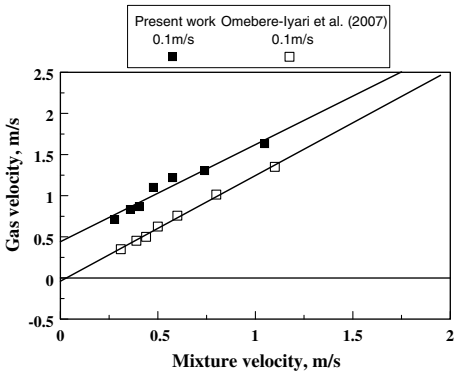

Fig. 15. Correlating drift flux parameters for the present work and the data of Omebere-Iyari et al. (2007). Liquid superficial velocity is given in legend.

4.2. Phase distribution

Fig. 16 shows that when the mean void fractions of the present steam/water data and the nitrogen/naphtha experiments of Omebere-Iyari et al. (2007) are equivalent, more fluctuations are observed in the former than in the latter. It is proposed that this is the consequence of a wider range of bubble sizes for the steam/water data and the presence of smaller and more uniform structures in the nitrogen/naphtha flow.

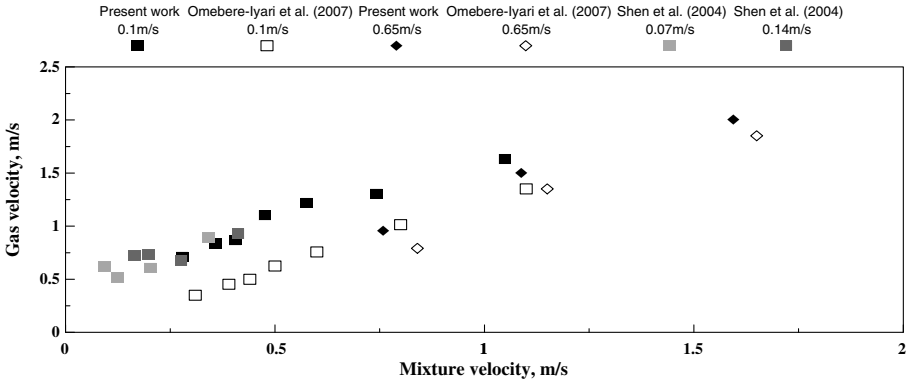

Fig. 14. Gas velocity versus mixture velocity for the present work, Omebere-Iyari et al. (2007) and Shen et al. (2004). Liquid superficial velocity is given in legend.

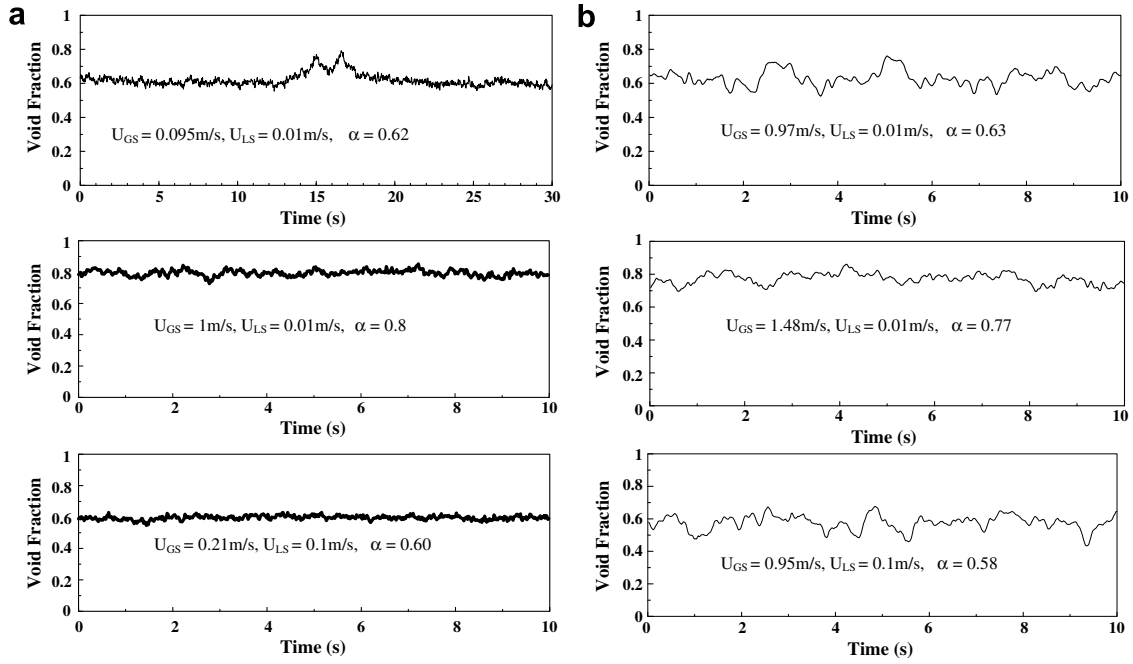

Fig. 16. Time varying, void fraction at similar mean void fractions for the data of Omebere-Iyari et al. (2007) (a) and the present work (b).

Although there are no local phase distribution data for the nitrogen/naphtha experiments conducted by Omebere-Iyari et al. (2007), it is possible to make inferences using the line and cross sectional averaged void fraction results by approximating the radial void fraction distribution with a simple power law relationship. Assuming that the radial void fraction is a function of the dimensionless radius, then

$$\varepsilon_r = \varepsilon_{rmax}(1 - r^{*y}) \tag{4}$$

where ε_r = radial void fraction, r^* = dimensionless radius, ε_{rmax} = maximum radial void fraction or magnitude factor and y = power law constant.

The line integral and area integral are given by $1 - \frac{1}{(y+1)}$ and $1 - \frac{2}{(y+2)}$ respectively. The line/area ratio is known for the nitrogen/naphtha data because line and cross-sectional averaged (or area) void fraction were measured. Hence, values of the power law constant, y, can be deduced. Mathematically, values of y equalling 1, 2 or infinity correspond to triangular, parabolic and perfectly flat profiles respectively.

For similar phase velocities in Fig. 17, the power law constants for the nitrogen/naphtha data of Omebere-Iyari et al. (2007) and present steam/water data are different. This suggests the existence of varying radial void fraction profiles for both sets of data. Eq. (4) is applied to both sets of data as shown in Fig. 18. The maximum value in the time varying void fraction is used as the magnitude factor. The agreement of radial void fraction profiles for the steam/water experiments, which are core peak distributions, with the proposed power law relationship is good. The value of the power law constant, y, is observed to be almost entirely in the range from 2 to 6 for core peak distributions (Fig. 17). The flat profiles predicted for the nitrogen/naphtha data could represent a wall peak distribution (which would require a more complex model) of which we have no proof. The present relationship therefore appears to give better predictions of the phase distribution at the pipe core than at the wall. In applying the power law relationship to the data from Shen et al. (2004), the power law constant is determined directly from Eq. (4) as no line void fraction data is provided. The resulting void fraction profiles obtained for the data of Shen et al. (2004) by inputting the power law constant to Eq. (4) (Fig. 18), confirm the existence of core peak profiles at the conditions investigated. This agrees with the present steam/water data. In addition to phase distribution, Fig. 19 shows that the void fraction observed in the present steam/water and the Shen et al. (2004) data are different from the nitrogen/naphtha experiments of Omebere-Iyari et al. (2007).

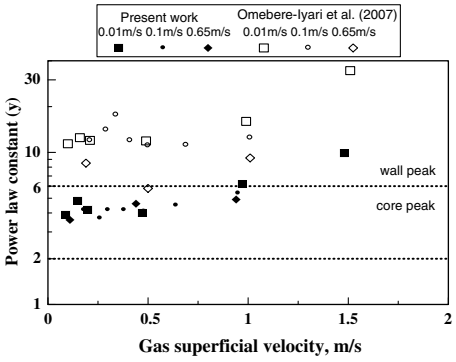

Fig. 17. Power law constants for estimation of radial void fraction profiles. Liquid superficial velocity is given in legend.

In the present work and in Omebere-Iyari et al. (2007) it is shown that the flow is fully developed at the measurement

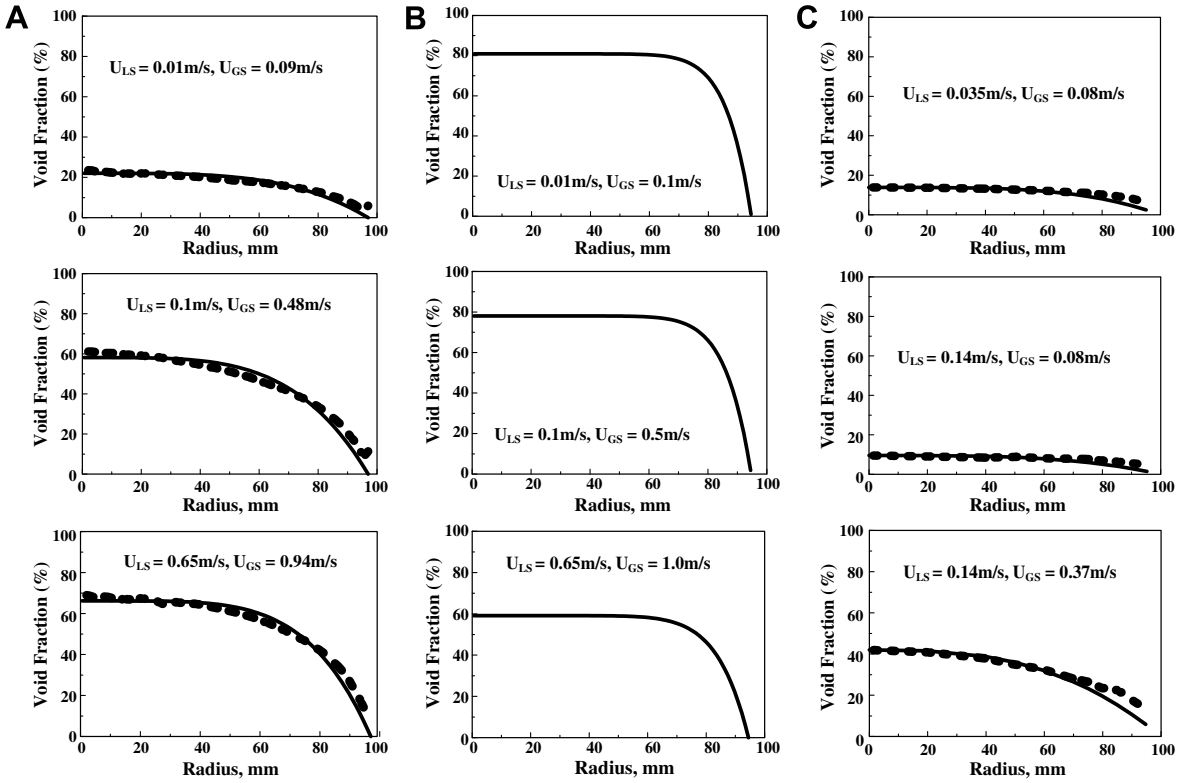

Fig. 18. Predicted and experimental radial profiles for the present work (A) and Shen et al. (2004) (C); approximated profile for the work of Omebere-Iyari et al. (2007) (B). Experimental data is represented by dotted line.

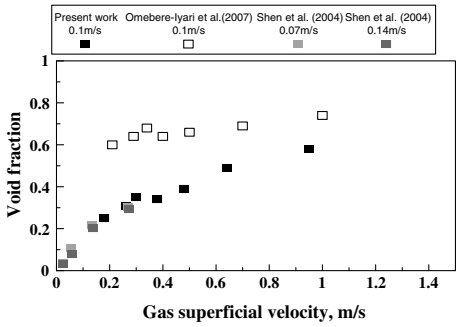

Fig. 19. Mean void fraction data for the present work, Omebere-Iyari et al. (2007) and Shen et al. (2004). Liquid superficial velocity in legend.

position for cross sectional void fraction. Shen et al. (2004) reports little effect of development length in their experiments. The different inlet mixing configurations employed by Omebere-Iyari et al. (2007) is shown by Omebere-Iyari and Azzopardi (2007) to give the same void fraction characteristics. The aforementioned findings eliminate development length or the inlet configuration as the reason for the differences between the present work and the work of Shen et al. (2004) with the data of Omebere-Iyari et al. (2007).

The effect of a multi-component liquid phase was examined using water with alcohols (Krishna et al., 2000; Camarasa et al., 1999) or sodium sulphate (Shäfer et al., 2002) or with mixtures of organic chemicals (Shäfer et al., 2002). The effect of the additive is to increase void fraction and the general consensus supported by work which has measured bubble sizes (Shäfer et al., 2002) is that this is achieved by inhibiting coalescence of bubbles. Naphtha being a liquid mixture of 66 hydrocarbon chemicals, therefore explains the high void fraction obtained by Omebere-Iyari et al. (2007) in sharp contrast to the much lower values observed in the present steam/water flow and the Shen et al. (2004) data, where a pure liquid is involved. The largest effect of system pressure usually appears as gas density. The gas density however, is equivalent for the nitrogen/naphtha data of Omebere-Iyari et al. (2007) and the present steam/water experiments and cannot therefore be responsible for the observed differences. Hence, the difference in other physical properties is the likely reason for the poor agreement between both sets of data. In this regard, evidence is found from the work of Lin et al. (1998) in bubble columns at elevated pressures. They observe that a significant reduction in surface tension and a substantial increase in liquid viscosity both decrease the maximum stable bubble size. The surface tension of the nitrogen/naphtha data is 25% less than that of steam/water and the liquid viscosity is greater by about 250%. This effect of fluid properties together with the effect of additives/liquid mixtures suggests that the steam/water flow is composed of larger bubbles than the nitrogen/naphtha flow and explains the smaller fluctuations in void fraction characteristics (Fig. 16) of the nitrogen/naphtha data.

Table 4
Flow pattern definitions in large diameter tubes

Flow pattern description	Flow pattern identification		
	Present work	Omebere-Iyari et al. (2007)	Ohnuki and Akimoto (2000)
Small bubbles in a liquid continuum	Bubble	Bubble	Undisturbed/agitated bubbly
Large coalescent bubbles which flow intermittently but do not occupy the entire pipe cross-section as Taylor bubbles	Churn-turbulent	absent	Churn-slug/froth
Developing process where bubble coalescence and disintegration occurs	absent	absent	Churn-bubbly
Intermittent regime consisting of two structures with high void fractions. In one, large bubbles are present and in the other smaller bubbles dominate	Absent	Intermittent	Absent

4.3. Flow pattern transitions

In Table 4, we attempt to establish common understanding by grouping two-phase flow patterns in large diameter risers with similar descriptions. For example, churn-turbulent flow in the present steam/water data is synonymous with churn-slug and churn-froth flow patterns in the work of Ohnuki and Akimoto (2000) and is not observed in the nitrogen/naphtha experiments of Omebere-Iyari et al. (2007).

Fig. 20 shows that the experimental bubble/churn-turbulent flow transition derived from the visualization studies differs from the bubble/slug flow transition predicted by Taitel et al. (1980) for the steam/water data. The model of Taitel et al. (1980) employs a constant critical void fraction for bubble flow of 0.25 for all pipe sizes. However, Omebere-Iyari and Azzopardi (2006) have shown that this value increases with pipe diameter assuming a constant bubble size.

The use of a critical void fraction for the bubble/slug flow transition of 0.38, which is the best estimate for the present steam/water experiments, in the Taitel et al. (1980) model, agrees with the bubble/churn-turbulent flow transition only at the highest liquid superficial velocity examined. The application of a critical voidage of 0.68, which was observed by Omebere-Iyari et al. (2007) in the naphtha/nitrogen tests, is in agreement with the lowest liquid superficial velocity. The failure of a constant critical void fraction with the Taitel et al. (1980) method to accurately predict the present bubble to churn-turbulent flow transition for the full range of liquid flow rates corroborates our observations regarding the absence of conventional slug flow. It also suggests that different mechanisms might be responsible for this transition. This may not be unconnected with the work of Ohnuki and Akimoto (2000), where a transition from bubbly to churn-froth flow occurs either directly or via an intermittent churn-bubbly regime which is characterized by a developing process with bubble coalescence and disintegration taking place.

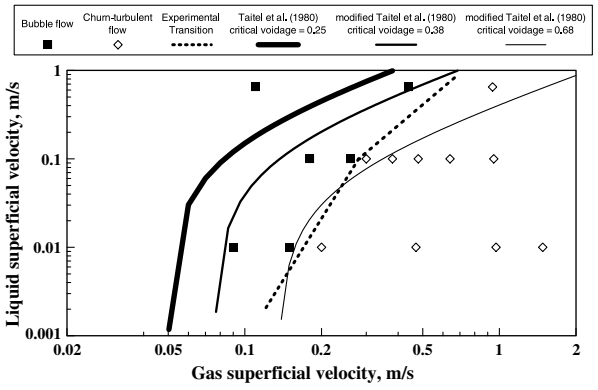

Fig. 20. Flow pattern transitions for the present steam/water data in a 194 mm diameter pipe at 46 bar.

5. Conclusions

From the work described in this paper, the following conclusions can be drawn:

(1) Steam/water flow at high pressure converges much quicker than air/water mixtures under atmospheric conditions.
(2) Slug flow, as defined for vertical two-phase flow systems to consist of a Taylor bubble occupying the whole pipe cross section and a liquid slug body, is absent in steam/water flows at high pressures in a large diameter tube.
(3) The void fraction of vertical two-phase flow involving steam/water and nitrogen/naphtha mixtures are very different for equivalent pipe diameters, liquid density and viscosity and phase velocities. This disparity is due to differences in liquid composition, which affects bubble coalescence (Shäfer et al., 2002).
(4) The smaller void fraction fluctuations in the Omebere-Iyari et al. (2007) data when compared to the steam/water test can be explained by Lin et al. (1998) who show that an increase in liquid viscosity and reduction in surface tension (a trend exhibited by naphtha over water) reduces maximum bubble size.
(5) The Probability Density Function plots for the present steam/water tests at high liquid velocities are different to those from the nitrogen/naphtha experiments of Omebere-Iyari et al. (2007) where negligible transformations in the void fraction PDF plots are observed as the flow pattern changes from bubble to annular flow.

(6) A simple power law relationship is used to predict core peak phase distribution profiles in two-phase flow systems. However, it appears that a more complex model is required for phase distributions at the pipe wall.
(7) The disparity in the drift velocities can be linked to the different phase distribution profiles for steam/water and nitrogen/naphtha flows. Mainly core peak profiles were obtained for steam/water flows while flatter profiles which may represent wall peak are predicted for the nitrogen/naphtha experiments of Omebere-Iyari et al. (2007).

Acknowledgements

The two-month stay of N.K. Omebere-Iyari at Rossendorf was made possible through the Business-Engineering and Science Travel Scholarship (BESTS) of the Roberts Money Postgraduate Training at the University of Nottingham and the kind support of the Institute for Safety Research, Forschungzentrum Dresden-Rossendorf.

"This work has been undertaken within the Joint Project on Transient Multiphase Flows. The Authors wish to acknowledge the contributions made to this project by the Engineering and Physical Sciences Research Council (EPSRC), the Department of Trade and Industry and the following: - Advantica; AspenTech; BP Exploration; Chevron; ConocoPhillips; ENI; ExxonMobil; FEESA; Granherne / Subsea 7; Institutt for Energiteknikk; Institut Français du Pétrole; Norsk Hydro; Petrobras, Scandpower; Shell; SINTEF; Statoil and TOTAL. The Authors wish to express their sincere gratitude for this support."

Appendix. Time and height averaging

For the present steam/water data, wire mesh sensor measurements are taken every 0.4 ms for 10 s over a negligible axial length. In the case of the gamma densitometers used by Omebere-Iyari et al. (2007), the height of the gamma beam in the flow as illustrated in Fig. 4 is significant (25–100 mm). An averaging technique to compensate for the different acquisition times and resolution heights of the wire mesh sensor and gamma densitometers is applied to make comparisons between the present work and the data of Omebere-Iyari et al. (2007). To obtain a measurement span for the wire mesh sensor that equates to the resolution height of the gamma densitometer, the relationship below is used:

$$h_{\text{gamma}} = U_{\text{gs}} \times t_{\text{wm}} \times n_{\text{wm}} \tag{5}$$

where gamma = gamma densitometer, wm = wire mesh sensor, t = acquisition time = 1/freq, freq = acquisition frequency, h = beam height, U_{gs} = gas superficial velocity and n = span (number of data acquisition cycles).

With n_{wm} determined, a moving average of the form shown below is applied

$$y_{\text{s}}(i) = \frac{1}{2N+1}(y(i+N) + y(i+N-1) + \ldots + y(i-N) \tag{6}$$

where $y_{\text{s}}(i)$ is the smoothed value for the ith data point, $2N+1$ is the span (n_{wm}) and N is the number of neighbouring data points on either side of $y_{\text{s}}(i)$. The Matlab *"smooth"* function is used to execute this procedure. When using the smooth function, the span must be odd; hence, n_{wm} will be approximated to the nearest odd integer. In addition, the data point to be smoothed must be at the center of the span. The span is adjusted for data points that cannot accommodate the specified number of neighbors on either side.

Every $\frac{freq_{\text{wm}}}{freq_{\text{gamma}}}^{\text{th}}$ data point from the wire mesh is averaged for time consistency with the gamma beam measurements.

References

Camarasa, E., Vial, C., Poncin, S., Wild, G., Midoux, N., Bouillard, J., 1999. Influence of coalescence behaviour of the liquid and of gas sparging on hydrodynamics and bubble characteristics in a bubble column. Chem. Eng. Process. 38, 329–344.

Cheng, H., Hills, J.H., Azzopardi, B.J., 1998. A study of the bubble to slug transition in vertical gas–liquid flow in columns of different diameter. Int. J. Multiphase Flow 24, 431–452.

Costigan, G., Whalley, P.B., 1997. Slug flow regime identification from dynamic void fraction measurements in vertical air–water flows. Int. J. Multiphase Flow 23, 263–282.

Hibiki, T., Ishii, M., 2000. Experimental study on hot-leg U-bend two-phase natural circulation in a loop with a large diameter pipe. Nucl. Eng. Des. 195, 69–84.

Kobayashi, A., Shakutsui, H., Mitsuyoshi, M., Minagwa, H., 2004. Void fraction in upward gas–liquid two-phase flow in a large diameter pipe. In: Proceedings of the 5th International Conference on Multiphase Flow, CD-ROM, #267.

Krishna, R., Urseanu, M.I., Dreher, A.J., 2000. Gas hold-up in bubble columns: influence of alcohol addition versus operation at elevated pressures. Chem. Eng. Process. 39, 371–378.

Kytomaa, H.K., Brennen, C.E., 1991. Small amplitude kinematic wave propagation in two-component media. Int. J. Multiphase Flow 17, 13–26.

Lin, T.-J., Tsuchiya, K., Fan, L.-S., 1998. Bubble flow characteristics in bubble columns at elevated pressure and temperature. Am. Inst. Chem. Eng. J. 44, 545–560.

Ohnuki, A., Akimoto, H., 2000. Experimental study on transition of flow pattern and phase distribution in upward air–water two-phase flow along a large vertical pipe. Int. J. Multiphase Flow 26, 267–286.

Okawa, T., Yoneda, K., Zhou, S., Tabata, H., 1999. New interfacial drag force model including effect of bubble wake, (II) Model validation using experimental data of steam-water bubbly flow in large-diameter pipes. J. Nucl. Sci. Technol. 36, 1030–1040.

Omebere-Iyari, N.K., Azzopardi, B.J., 2006. The effect of pipe diameter and pressure in vertical gas/liquid upflow. In: 4th Japanese–European Two-Phase Flow Group Meeting.

Omebere-Iyari, N.K., Azzopardi, B.J., 2007. Gas/liquid flow in a large riser: effect of upstream configurations. In: 13th International Conference on Multiphase Production Technology pp. 5–15.

Omebere-Iyari, N.K., Azzopardi, B.J., Ladam, Y., 2007. The identification of two-phase flow patterns and their transitions in large diameter vertical pipes at elevated pressures. Am. Inst. Chem. Eng. J. 53, 2493–2504.

Pietruske, H., Prasser, H.-M., 2005. Wire-mesh sensors for high-resolving two-phase flow studies at high pressures and temperatures. In:

Proceedings of the 11th International Topical Meeting on Nuclear Reactor Thermal-Hydraulics, CD-ROM, #533.

Prasser, H.-M., 2004. Influence of the gas injection on the void fraction profiles and bubble size distributions of an air–water flow in vertical pipes. In: 5th International Conference on Multiphase Flow, CD-ROM, #187.

Prasser, H.-M., Bottger, A., Zschau, J., 1998. A new electrode-mesh tomograph for gas–liquid flows. Flow Measur. Instrument. 9, 111–119.

Prasser, H.-M., Scholz, D., Zippe, C., 2001. Bubble size measurement using wire-mesh sensors. Flow Measur. Instrument. 12, 299–312.

Prasser, H.-M., Krepper, E., Lucas, D., 2002. Evolution of the two-phase flow in a vertical tube – decomposition of gas fraction profiles according to bubble size classes using wire-mesh sensors. Int. J. Therm. Sci. 41, 17–28.

Prasser, H.-M., Beyer, M., Bottger, A., Carl, H., Lucas, D., Schaffrath, A., Schutz, P., Weiss, F.P., Zschau, J., 2005a. Influence of the pipe diameter on the structure of the gas–liquid interface in a vertical two-phase pipe flow. Nucl. Technol. 152, 3–22.

Prasser, H.-M., Beyer, M., Carl, H., Gregor, S., Manera, A., Pietruske, H., Schutz, P., Weiss, F.P., 2005b. TOPFLOW: design, results and perspectives. Annual Report 2004, Institute of Safety Research, Forschungzentrum Dresden-Rossendorf, pp. 3–14.

Prasser, H.-M., Beyer, M., Carl, H., Gregor, S., Lucas, D., Pietruske, H., Schutz, P., Weiss, F.P., 2005c. Evolution of the structure of a gas–liquid two-phase flow in a large vertical pipe. In: Proceedings of the 11th International Topical Meeting on Nuclear Reactor Thermal-Hydraulics, CD-ROM, #399.

Shäfer, R., Merten, C., Eigenberger, G., 2002. Bubble size distributions in a bubble column reactor under industrial conditions. Exp. Therm. Fluid Sci. 26, 595–604.

Shen, X., Mishima, K., Nakamura, H., 2004. Two-phase phase distribution effect on drift flux parameters in a vertical large diameter pipe. Two-Phase Flow Modell Exp. 2, 1059–1066.

Shoukri, M., Hassan, I., Gerges, I.E., 2003. Two-phase bubbly flow structure in large-diameter vertical pipes. Can. J. Chem. Eng. 81, 205–211.

Taitel, Y., Barnea, D., Dukler, A.E., 1980. Modelling flow pattern transitions for steady upward gas–liquid flow in vertical tubes. Am. Inst. Chem. Eng. J. 26, 345–354.

Yoneda, K., Yasuo, A., Okawa, T., 2002. Flow structure and bubble characteristics of steam-water two-phase flow in a large-diameter pipe. Nucl. Eng. Des. 217, 267–281.

Zhu, W., Ching C., Shoukri, M., 2004. Phase distribution and flow regime transition of two-phase flow in large diameter pipes. In: Proceedings of the 5th International Conference on Multiphase Flow, CD-ROM, #399.

Zuber, N., Findlay, J.A., 1965. Average volumetric concentration in two-phase flow systems. Trans. ASME: J. Heat Transfer 87, 453–468.